Structure
Article

Recognition of Mono-ADP-Ribosylated ARTD10 Substrates by ARTD8 Macrodomains

Alexandra H. Forst,[1] Tobias Karlberg,[2] Nicolas Herzog,[1] Ann-Gerd Thorsell,[2] Annika Gross,[1] Karla L.H. Feijs,[1] Patricia Verheugd,[1] Petri Kursula,[3,4] Bianca Nijmeijer,[5,6] Elisabeth Kremmer,[7] Henning Kleine,[1,8] Andreas G. Ladurner,[5,6] Herwig Schüler,[2,*] and Bernhard Lüscher[1,*]

[1]Institute of Biochemistry and Molecular Biology, Medical School, RWTH Aachen University, 52057 Aachen, Germany
[2]Structural Genomics Consortium and Department of Medical Biochemistry and Biophysics, Karolinska Institutet, Scheeles väg 2, 17177 Stockholm, Sweden
[3]Department of Biochemistry and Biocenter Oulu, University of Oulu, 90014 Oulu, Finland
[4]Centre for Structural Systems Biology-Helmholtz Centre for Infection Research and Department of Chemistry, University of Hamburg, DESY, 22607 Hamburg, Germany
[5]European Molecular Biology Laboratory, Gene Expression Unit, Meyerhofstrasse 1, 69117 Heidelberg, Germany
[6]Butenandt Institute of Physiological Chemistry, University of München, Butenandtstrasse 5, 81377 München, Germany
[7]Helmholtz Zentrum München, Institute of Molecular Immunology, Marchioninistr. 25, 81377 München, Germany
[8]Present address: Abbott GmbH & Co. KG, Max-Planck-Ring 2a, 65205 Wiesbaden, Germany
*Correspondence: herwig.schuler@ki.se (H.S.), luescher@rwth-aachen.de (B.L.)
http://dx.doi.org/10.1016/j.str.2012.12.019

SUMMARY

ADP-ribosyltransferases (ARTs) catalyze the transfer of ADP-ribose from NAD^+ onto substrates. Some ARTs generate in an iterative process ADP-ribose polymers that serve as adaptors for distinct protein domains. Other ARTs, exemplified by ARTD10, function as mono-ADP-ribosyltransferases, but it has been unclear whether this modification occurs in cells and how it is read. We observed that ARTD10 colocalized with ARTD8 and defined its macrodomains 2 and 3 as readers of mono-ADP-ribosylation both in vitro and in cells. The crystal structures of these two ARTD8 macrodomains and isothermal titration calorimetry confirmed their interaction with ADP-ribose. These macrodomains recognized mono-ADP-ribosylated ARTD10, but not poly-ADP-ribosylated ARTD1. This distinguished them from the macrodomain of macroH2A1.1, which interacted with poly- but not mono-ADP-ribosylated substrates. Moreover, Ran, an ARTD10 substrate, was also read by ARTD8 macrodomains. This identifies readers of mono-ADP-ribosylated proteins, defines their structures, and demonstrates the presence of this modification in cells.

INTRODUCTION

Protein ADP-ribosylation regulates diverse processes including chromatin remodeling, transcription control, DNA repair, and signaling (Gibson and Kraus, 2012; Hottiger et al., 2010). The ''writers'' are mono- and poly-ADP-ribosyltransferases (ARTs) that modify specific protein targets. Recent studies demonstrate that poly-ADP-ribose (PAR) synthesized by ARTD1/PARP1 (see Hottiger et al., 2010 for definition of new nomenclature) and ARTD5 (Tankyrase) serve as protein-binding sites. For example, ARTD1, activated and PARylated in response to DNA damage, recruits DNA repair proteins through PAR-binding macrodomains and PBZ domains (Ahel et al., 2008; Eustermann et al., 2010; Gottschalk et al., 2009; Karras et al., 2005; Kleine and Lüscher, 2009; Timinszky et al., 2009). Furthermore, the ubiquitin E3 ligase RNF146/Iduna interacts with several PARylated proteins via its WWE domain, resulting in RNF146 activation and ubiquitination of the PARylated proteins (Kang et al., 2011). As an example, ARTD5 PARylates axin, a key scaffold protein in the WNT signaling pathway, which recruits RNF146 (Callow et al., 2011; Huang et al., 2009; Zhang et al., 2011). 3BP2 is also substrate of ARTD5 that subsequently becomes substrate of RNF146. 3BP2 mutants that are unable to interact with ARTD5 are associated with cherubism (Guettler et al., 2011; Levaot et al., 2011). RNF146 was also found to protect neuronal cells from glutamate excitotoxicity dependent on its ability to interact with PAR (Andrabi et al., 2011). Thus, interaction of different proteins to PAR controls local protein concentration and affects the activities of binding partners, which are key consequences downstream of the activation of PAR-forming ARTDs.

Whereas macrodomains are also capable of binding to ADP-ribose (ADPr), WWE and PBZ domains require the α-(1″–2′) *O*-glycosidic bond present in PAR for efficient interaction (Eustermann et al., 2010; Karras et al., 2005; Wang et al., 2012). A short linear peptide motif consisting of hydrophobic and basic amino acids binds also to PAR. This motif was identified in several proteins, often related to DNA damage and repair, transcription, replication, and chromatin structure (Gagné et al., 2008; Kleine and Lüscher, 2009; Pleschke et al., 2000). Thus, PAR and its reader modules mediate protein-protein interactions.

Several ARTD enzymes, exemplified by the MYC-binding partner ARTD10 (Yu et al., 2005), function as mono-ADP-ribosyltransferases in vitro (Di Paola et al., 2012; Kleine et al., 2008). However, it is still unclear whether ARTD-mediated mono-ADP-ribosylation (MARylation) exists in cells, although

the analysis of catalytically inactive mutants suggests a functional role of MARylation (Kleine et al., 2008). Several studies have indicated MARylation of specific cellular proteins using mainly indirect means and permeabilized cells, leaving open whether extracellular mono-ADP-ribosyltransferases of the ARTC family were involved in the modification (Dani et al., 2009, 2011; Koch-Nolte et al., 2008; Lupi et al., 2000). The macrodomain of Af1521 from *Archaeoglobus fulgidus* was used to detect potentially MARylated proteins, but Af1521 also binds to PAR (Dani et al., 2009; Guetg et al., 2012; Karras et al., 2005). Moreover, it remains unclear whether intracellular reader domains for MARylated substrates exist. Previously, macrodomains were found to interact with free ADPr and with *O*-acetyl-ADP-ribose, the product of deacetylation reactions catalyzed by sirtuins, in addition to binding to PAR (Chen et al., 2011). Structural analyses of different macrodomains revealed a highly conserved ADPr-binding domain (Chen et al., 2011; Hassler et al., 2011; Karras et al., 2005; Timinszky et al., 2009). However, no structures of a macrodomain associated with an ADP-ribosylated substrate are presently available. Reasons include that PARylated substrates are heterogeneous and that MARylated substrates are presently not available. Within the ARTD family, ARTD8 (BAL2/PARP14), originally identified as B cell-aggressive lymphoma (BAL) protein (Aguiar et al., 2000), contains three macrodomains and a WWE domain besides the ADP-ribosyltransferase domain (see Figure 1A) (Aguiar et al., 2005). Similar to ARTD8, ARTD9/BAL-1 and ARTD7/BAL-3 combine macrodomains with ADP-ribosyltransferase domains (Aguiar et al., 2000; Hottiger et al., 2010). Because ARTD8 is a mono-ADP-ribosyltransferase (Kleine et al., 2008), we hypothesized that a link might exist between the ARTD8 macrodomains and MARylation. Therefore, we addressed whether the ARTD8 macrodomains interact with ADPr and whether these domains serve as binding modules for MARylated substrates.

We found that ARTD8 macrodomains specifically interacted with mono-ADP-ribosylated substrates modified by ARTD10 both in vitro and in cells, providing formal evidence that endogenous MARylation exists in cells. The structure of these macrodomains revealed a conserved fold for ADPr binding, similar to other macrodomains. Despite this similarity, ARTD8 macrodomains do not interact with ADPr polymers, indicating that distinct macrodomains read either MARylated or PARylated.

RESULTS

ARTD8 Macrodomains Bind Mono-ADP-Ribosylated ARTD10

Although the ARTD10 mono-ADP-ribosyltransferase activity is well documented in vitro (Kleine et al., 2008), it is less clear whether MARylation by intracellular enzymes occurs in cells. We noticed that ARTD10 colocalized with murine Artd8 in cells upon transient expression (Figure 1B). Artd8 contains a WWE domain and three macrodomains (Macro1–3) that might mediate a possible interaction (Figure 1A). Homologs of both domains have been shown to bind to PAR (Callow et al., 2011; Gottschalk et al., 2009; Kang et al., 2011; Timinszky et al., 2009; Zhang et al., 2011). Pull-down experiments revealed that Macro1–3, but not Macro1 alone, nor the WWE domain, bound automodified but not unmodified ARTD10 (Figure 1C). Binding was specific and dependent on β-NAD^+ levels (Figure S1 available online), suggesting that MARylation of ARTD10 is a prerequisite for binding. In addition to Macro1–3, Macro2 and Macro3 also interacted with automodified ARTD10 (Figure 1D). Similar results were obtained with the macrodomains of human ARTD8 (Figure S1B). The specificity of the interaction was further highlighted by the absence of detectable binding of ARTD10(1–255) (Figure 1D), which cannot be MARylated (Kleine et al., 2008). Also, the macrodomain of histone macroH2A1.1 and its binding-deficient mutant (G224E/F348A) did not interact with ARTD10 (Figure 1E), but histone macroH2A1.1-bound PARylated ARTD1 as expected (Figure 1F) (Timinszky et al., 2009). In contrast, the Artd8 macrodomains were unable to bind PARylated ARTD1 (Figure 1F). This indicates that specific macrodomains bind either mono- or poly-ADP-ribosylated substrates.

We further validated the importance of ARTD10 MARylation for its interaction with the Artd8 macrodomains. Macro1–3 was unable to bind the catalytically inactive mutant ARTD10-G888W (Figure 2A), and binding was substantially reduced when the automodification reaction was performed in the presence of the ART inhibitor benzamide (Figure S1C). Finally, the interaction with MARylated ARTD10 was subject to competition by ADPr (Figures 2B and S1D). To address the specificity of the macrodomains, we introduced the G1055E mutation into Macro2. Mutation of the corresponding residue in the macrodomain of Af1521 interfered with ADPr binding (Dani et al., 2009). This single amino acid exchange was sufficient to abrogate binding to ARTD10 (Figure 2C).

Architecture of ARTD8 Macrodomains

To further evaluate the specific ADPr-binding ability of ARTD8's macrodomains, we solved the crystal structure of a protein construct encompassing human ARTD8 macrodomains 1 and 2 (referred to as Macro1–2, residues Gly784–Ser1196) (Figure 3A; Table 1). Each domain contained a central seven-stranded β sheet flanked by two or three α helices on each side. The individual domains packed tightly together forming an interface of 906 $Å^2$. The two domains interacted through 11 hydrogen bonds and salt bridges as well as several hydrophobic contacts (Figure 3B). The complementary charges of their surfaces were clearly visible in electrostatic surface potential maps (Figure 3C).

The affinities of each domain for ADPr were determined using isothermal titration calorimetry (ITC). Macro1 bound free ADPr with low affinity and Macro2 and 3 with high affinity (Tables 2 and S1; Figure S2), consistent with our pull-down experiments shown above (Figure 1). For each particular domain, we determined similar binding constants regardless of whether single-, tandem-, or triple-domain constructs were used (Table 2), indicating that the individual domains did not cooperate. Thus, ARTD8 macrodomains are ADPr-binding modules that do not stand in allosteric contact with one another.

We determined the crystal structures of all three individual ARTD8 macrodomains and also of ARTD7-Macro2 in complex with ADPr (Figure 4; Table 1). Pairwise superposition showed that all structures are very similar (Figure 4A): ARTD8-Macro3 and ARTD7-Macro2 (~60% protein sequence identity) align to a root mean square difference of 0.69 Å in C_α-atom positions, whereas all other combinations of structures (10%–30% identity)

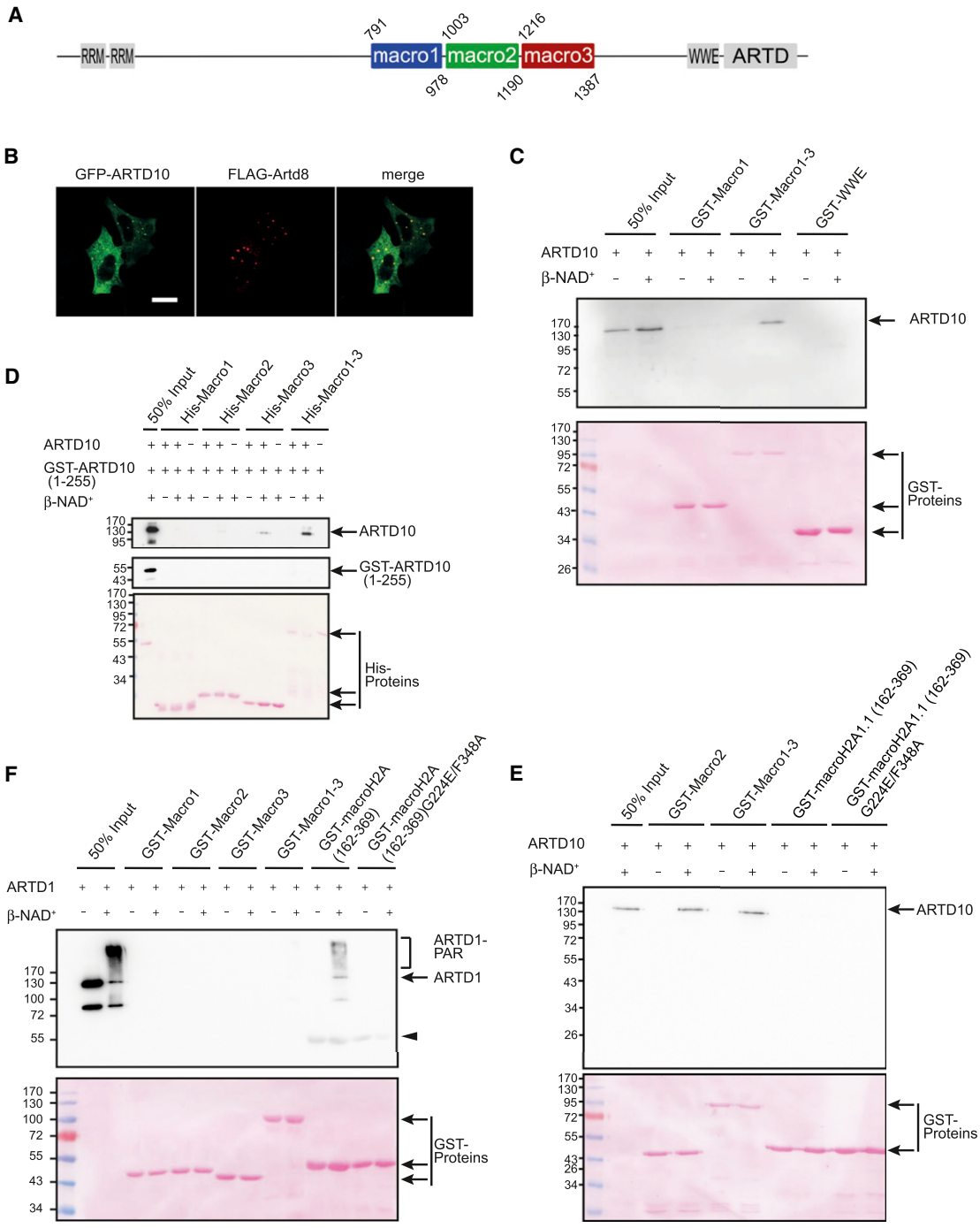

Figure 1. Artd8 Macrodomains Interact with Mono-ADP-Ribosylated ARTD10

(A) Schematic representation of the ARTD8 domain architecture. Residue numbers refer to the human ortholog.

(B) EGFP-ARTD10 and FLAG-Artd8 were transiently coexpressed in HeLa cells. The cells were fixed, stained with FLAG-specific antibodies (red), and analyzed by confocal microscopy. Scale bar, 20 μM.

(C) Purified ARTD10 was automodified in the presence or absence of 500 μM β-NAD$^+$ and subsequently incubated with the indicated bacterially expressed GST-tagged Artd8 macrodomain or WWE domain. The complexes bound to glutathione Sepharose were analyzed by western blot analysis using ARTD10-specific polyclonal antibodies (upper panel). For control, all blots were stained with Ponceau red.

(D) ARTD10 was incubated as in (C) and bound to bacterially expressed hexahistidine-tagged macrodomains of Artd8. The complexes were recovered on TALON beads and analyzed by western blot analysis using ARTD10-specific polyclonal antibodies (upper panel). The ADP-ribosylation reaction contained 5 μg of GST-ARTD10(1–255), which was detected using GST-specific antibodies (middle panel).

(E) The experimental setup was as in (C) with the exception that GST-tagged mouse macroH2A1.1(126–369), encoding the macrodomain, and a mutant were used in addition to the macrodomains of Artd8.

(legend continued on next page)

aligned to between 1.3 and 1.6 Å. A structure-based sequence alignment is presented in Figure S3.

All of our macrodomain-ADPr complex structures display the ligand well defined in the electron density maps (Figure 4B). ADPr is bound in a deep surface groove on the "crest" of the domain (Figure 4C), the outline of which is formed by two tight turns and three extended loops (designated I–V in Figure 4D). These loops appear more flexible than the overall domains, as judged by higher experimental B factors. Comparison of an *apo* structure of Macro3 and its ADPr complex reveals that these loops open up slightly to accommodate the ligand (Figure S4). The central part of the groove binds the pyrophosphates by conserved interactions mainly with backbone atoms from extended loops II and IV (Figures 4D–4F).

An aspartate side chain in loop V, which forms a hydrogen bond with the adenine base nitrogen N6, was essential for ADPr binding by the macrodomain of histone macroH2A1.1 (Figure 4G) (Kustatscher et al., 2005). Our crystal structures show that aspartate side chains fulfill the same function in Macro3 and in ARTD7-Macro2; by contrast, in Macro2, a nonconserved glutamine (Gln1024 in loop I) hydrogen bonds with the adenine N6 in a similar geometry. In Macro1, this interaction is entirely missing because the base moiety is tilted out of the pocket away from loop I (Figure 4D). Interactions between protein and adenosine base are most extensive in Macro3, where the hydrogen bond with Asp1235 is complemented by a base-stacking interaction with the Phe1371 side chain (Figure 4F). Base stacking to a phenylalanine is also conserved in histone macroH2A1.1 (Figure 4G) and ARTD7-Macro2; in Macro2, this position is occupied by a histidine (Figure 4E). Together, these differences in adenine base binding may be sufficient to explain the differences in ligand affinities, in particular the notably weaker affinity of Macro1 for ADPr (Table 2) and MARylated ARTD10 (Figures 1D and 1E). The positions and orientations of the adenine ribose and of the central pyrophosphates are similar in all ARTD8 and ARTD7 macrodomain structures.

Active ARTD10 and the Macrodomains of Artd8 Interact in Cells

Next, we investigated whether protein MARylation can be detected in cells. Therefore, HeLa cells stably expressing inducible ARTD10 or ARTD10-G888W were transiently transfected with plasmids encoding EGFP-tagged Artd8 macrodomains, and immunofluorescence imaging was performed. ARTD10 accumulates in dot-like structures (Kleine et al., 2012). As soon as the ARTD10 dots became visible, EGFP-Macro1–3, but not EGFP alone, colocalized with these dots (Figure 5A). In contrast, no colocalization between EGFP-Macro1–3 and the catalytically inactive ARTD10-G888W was observable. EGFP-Macro2 and EGFP-Macro3, but not EGFP-Macro1 and EGFP-Macro2-G1055E, also colocalized with ARTD10, but not with ARTD10-G888W (Figure S5). These findings were complemented by coimmunoprecipitation experiments in HEK293 cells. Macro1–3 and Macro2, but not Macro2-G1055E, were capable to bind ARTD10 (Figure 5B). This demonstrated that Artd8 macrodomains interact with ARTD10 in cells, providing evidence for catalytic activity of intracellular ARTD10.

To exclude contributions of PAR-synthesizing ARTDs to the interaction between ARTD10 and Artd8's macrodomains in cells, we conducted coimmunoprecipitation experiments in the presence of Olaparib and IWR-1, which collectively inhibit ARTD1–ARTD6 (Chen et al., 2009; Wahlberg et al., 2012). Indeed, activation of ARTD1 was efficiently inhibited under these conditions (Figure S6). Nonetheless, binding of EGFP-Macro1–3 to ARTD10 was not influenced (Figure 5C), suggesting that PARylation does not play a role for the interaction.

Next, we investigated whether endogenous ARTD10 interacts with the macrodomains of Artd8. Because HEK293 and HeLa cells express only low amounts of ARTD10, we chose U2OS cells. In these cells, IFN-α stimulates the *ARTD10* promoter (A.G., P.V., and B.L., unpublished data; Mahmoud et al., 2011), allowing detection of endogenous ARTD10 protein (Figure 6A). It also accumulated in dot-like structures that were more prominent upon IFN-α stimulation, some of which were stained with EGFP-tagged Macro1–3 (Figures 6A and 6B). Compared to the overexpressed ARTD10, the ratio of colocalizing dots was reduced, suggesting that ARTD10 was only active in some of the dots (Figures 5 and 6).

In the presence of IWR-1 and Olaparib, consistent with the coimmunoprecipitation experiments, colocalization between endogenous ARTD10 and EGFP-Macro1–3 was not impaired (Figures 6C, 6D, and S7A). Similarly, colocalization in the presence of the inhibitors was observed in HeLa cells that stably express inducible ARTD10 (Figure S7B). No colocalization of ECFP-macroH2A1.1(162–369) with endogenous ARTD10 dots was detected (Figure S8). Thus, the macrodomains of Artd8 specifically recognize MARylated ARTD10 in cells.

Artd8 Macrodomains Bind Mono-ADP-Ribosylated GTP-Bound RAN

Macrodomains of ARTD8 recognize ADP-ribosylated ARTD10 both in vitro and in cells, but not the unmodified protein. We were now interested to evaluate whether any ARTD10 substrate could be detected by macrodomains. Previously, we identified core histones as in vitro substrates of ARTD10 (Kleine et al., 2008). However, because core histones are known substrates for ARTD1/PARP1, we decided to study other substrates. Because many bacterial ADP-ribosylating toxins target small GTPases (Di Girolamo et al., 2005), we tested whether the GTPases RhoA, Ras, or Ran were substrates of ARTD10. Of these proteins, only Ran-GppNHp was specifically modified by ARTD10 (Figure 7A). Notably, binding of the nonhydrolyzable GTP analog GppNHp to Ran induces a large conformational change in the protein (Vetter et al., 1999), suggesting that this structural change is a prerequisite for Ran modification by ARTD10.

Next, we determined whether MARylated Ran-GppNHp is recognized by macrodomains. Pull-down experiments demonstrated that Ran-GppNHp interacted with His-Macro1–3 or

(F) Purified ARTD1 was automodified in the presence or absence of 500 μM β-NAD^+ and subjected to a pull-down assay with bacterially expressed GST-tagged macrodomains of Artd8, GST-tagged macroH2A1.1(162–369), or macroH2A1.1(162–369)G224E/F348A. Bound proteins were analyzed by western blotting using ARTD1-specific polyclonal antibodies. The arrowhead identifies a nonspecific band.
See also Figure S1.

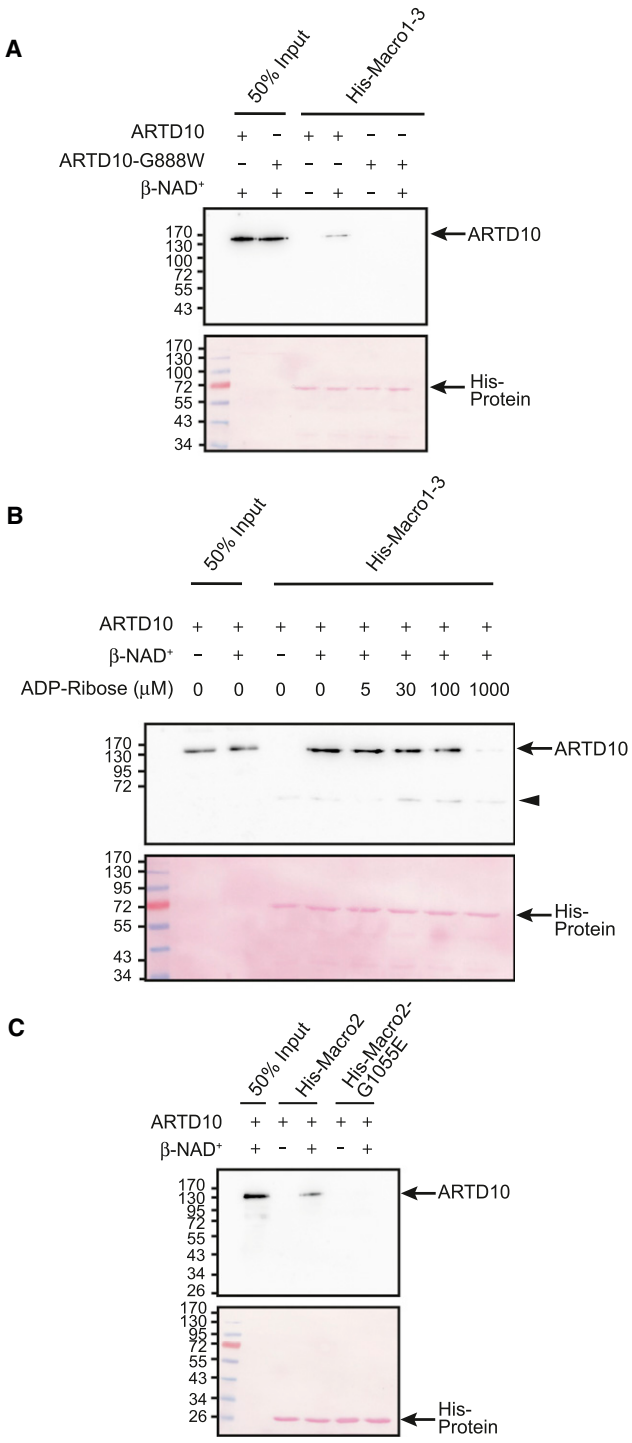

Figure 2. Specificity of the Interaction between Mono-ADP-Ribosylated ARTD10 and the Macrodomains of Artd8

(A) Purified ARTD10 and ARTD10-G888W were incubated in the presence or absence of 500 μM β-NAD+. Binding of ARTD10 proteins to hexahistidine-tagged Macro1–3 was measured by western blot analysis using ARTD10-specific polyclonal antibodies (upper panel). For control, the blot was stained with Ponceau red (lower panel).

(B) The experimental setup was as in (A). Automodified ARTD10 and His-Macro1–3 were incubated in the presence of increasing amounts of ADPr. The arrowhead identifies a nonspecific band.

(C) The experimental setup was as in (A). Binding of ARTD10 was measured to His-Macro2 or His-Macro2-G1055E, a mutant that is unable to bind to ADPr. See also Figure S1.

His-Macro3 when modified by ARTD10 (Figures 7B and 7C). Incubation of Ran-GppNHp with ARTD10 in the absence of β-NAD+ or with ARTD10-G888W did not result in macrodomain binding. Thus, MARylated Ran is specifically recognized by macrodomains. To evaluate whether Ran is MARylated in cells, HA-ARTD10 and HA-ARTD10-G888W were transiently expressed in HEK293 cells together with EGFP-tagged Artd8 macrodomains. Ran was coimmunoprecipitated with EGFP-Macro1–3 and to a lesser extent with EGFP-Macro3 in the presence of ARTD10 but not the catalytically inactive mutant (Figure 7D). Together, these findings provide evidence that in cells, Ran is an ARTD10 substrate that, if ADP-ribosylated, is recognized by Artd8 macrodomains.

DISCUSSION

Of the 17 protein ADP-ribosyltransferases (ARTDs) that exist in mammalian cells (Hottiger et al., 2010), 9 have documented or suggested MARylation activity (Kleine et al., 2008). Although PAR formed by ARTD1 has been well documented by using specific antibodies, it was unclear whether MARylation by ARTDs occurs in cells due to the lack of suitable tools. We now demonstrate that ARTD8 macrodomains are ADPr-binding modules that detect ARTD10-dependent MARylated substrates both in vitro and in cells. Thus, we provide formal evidence that MARylation by an endogenous enzyme of the ARTD family indeed exists in mammalian cells. Together, these findings strongly suggest that MARylation is an intracellular posttranslational modification that contributes to protein interaction and crosstalk.

The specificity of the different ARTDs is only poorly understood, and we cannot exclude the possibility that MARylated substrates become available to polymer-forming enzymes in cells. Moreover, PAR glycohydrolase (PARG), the enzyme responsible for the majority of PAR breakdown in cells, cleaves PAR but appears to be unable to remove the final ADPr unit linked to the protein (Slade et al., 2011). Thus, transitions between mono- and poly-ADP-ribosylation might occur on potentially any given ARTD substrate. Hence, it was important to establish evidence for the existence of MARylation in cells and of domains that can distinguish between MAR and PAR. Macro2 and Macro3 of Artd8 are such domains:

(1) Although Macro2 and Macro3 interacted with MARylated but not PARylated substrates, the macrodomain of macroH2A1.1, a reported PAR binder (Timinszky et al., 2009), showed the reverse-binding specificity (Figures 1 and S8). If MARylated ARTD10 were substrate of polymer-forming ARTDs and thus were PARylated, we would have expected colocalization with the macrodomain of macroH2A1.1.

(2) Only one distinct band of ARTD10 was coimmunoprecipitated by Macro1–3 (Figure 5B). If ARTD10 was PARylated in cells, we would have anticipated a more

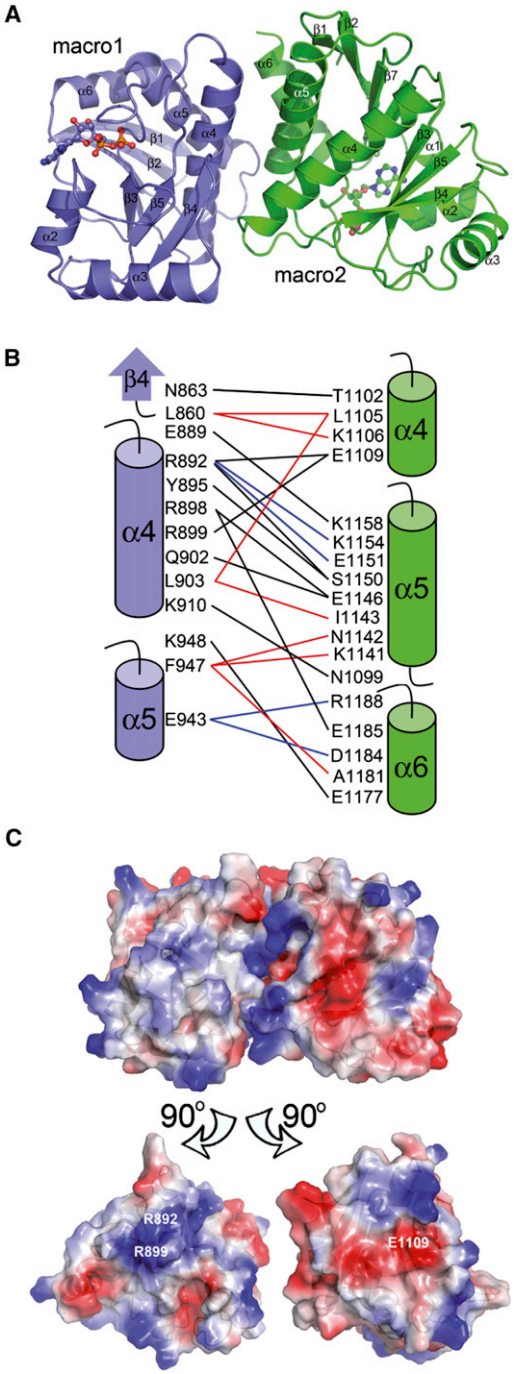

Figure 3. Crystal Structure of the ARTD8 Macrodomains

(A) Crystal structure of a human ARTD8 Macro1 and Macro2 protein fragment. ADPr-binding sites on opposite sides of the two-domain protein are indicated.

(B) Cartoon of the side chains that contribute to the interface between ARTD8 Macro1 (blue) and Macro2 (green). Water-mediated interactions are indicated by blue lines, other polar interactions by black lines, and nonpolar interactions by red lines.

(C) Surface rendering of calculated electrostatic potential, where red indicates acidic and blue indicates basic sites. In the lower panel, the interface is shown exposed by rotation of domains 1 and 2 by 90° to the left and right, respectively, to illustrate matching buried surface charges.

See also Figure S3 and Table S2.

diffuse band for PARylated ARTD10 due to the heterogeneous nature of ADPr polymers, rather than a single protein band.

(3) Inhibition of ARTD1–ARTD4 by Olaparib and of ARTD5–ARTD6 by IWR-1 did not influence the binding of Artd8's macrodomains to MARylated ARTD10 in cells (Figures 5C, 6B, and S7).

(4) Macro2 and Macro3, shown to be robust binders of MARylated substrates of ARTD10 (Figures 1D, 1E, and 7), displayed no interaction with PARylated ARTD1 (Figure 1F).

Of note, human MacroD1 protein was recently shown to have *O*-acetyl-ADP-ribose deacetylase activity (Chen et al., 2011). Also, the catalytic domain of PARG possesses a macrodomain fold (Slade et al., 2011). Moreover, and as discussed above, macrodomains are interaction modules of PAR (Gibson and Kraus, 2012). These findings suggest that macrodomains are intimately involved in ADPr biology and metabolism. Contrasting PARG, we were unable to detect hydrolyzing activity of any of the Artd8 macrodomains. In support, our crystal structures show that none of the ARTD8 macrodomains features acidic side chains that could serve to activate N-ribose hydroxyls for nucleophilic attack (Figures 3D–3F). In addition, the interactions of these macrodomains with MARylated ARTD10 and Ran as seen in the pull-down and coimmunoprecipitation experiments (Figures 1, 2, 5, and 7) are consistent with a lack of hydrolyase activity. Thus, the three ARTD8 macrodomains are unable to reverse MARylation of ARTD10. Together, our findings strongly suggest that distinct macrodomains, despite their common ability to bind free ADPr, possess specificity for binding to either MARylated or PARylated substrates. In addition, some have catalytic activity, defining macrodomains as key modules in processing ADP-ribosylation (Figure 8).

Differential specificity of distinct macrodomains is also supported by our crystal structures. These revealed different conformations of the N-ribose, which are in local environments where nonconserved side chains might contribute to the binding sites of putative ADP-ribosylated target proteins. Also, α3 of ARTD8-Macro3 is shorter by two helical turns than the corresponding helices in any other macrodomain structure, resulting in a more exposed site near the N-ribose (Figure 4F). These observations underscore the general structural variability at this position, which is consistent with target protein recognition sites in proximity to the N-ribose. Although differences can be noticed, it is important to point out that presently, no structures of a macrodomain with an ADP-ribosylated substrate protein are available. Thus, it remains unclear how macrodomains are able to distinguish between MARylated and PARylated substrates.

Thus far, the automodification sites within ARTD10 are not known, except for E882 (Kleine et al., 2008). However, it is likely that more than one site exists, similar to the findings with other members of the ARTD family (Altmeyer et al., 2009; Tao et al., 2009). Taking the possibility of several automodification sites into account, this might explain the observation that the interaction between ARTD10 and Macro1–3 was often apparently stronger than between ARTD10 and either Macro2 or Macro3 alone (Figure 1). Furthermore, the existence of more than one

Table 1. Data Collection, Phasing, and Crystallographic Refinement Statistics

Data Collection	ARTD8m1 (ADPr)	ARTD8m2 (ADPr)	ARTD8m3 (apo)	ARTD8m3 (ADPr)	ARTD8m12 (ADPr)	ARTD8m12 (ADP)	ARTD7m2 (ADPr)
PDB	3Q6Z	3Q71	4ABL	4ABK	3VFQ	4D86	3V2B
Synchrotron	BESSY	MAX-II	DIAMOND	BESSY	ESRF	BESSY	BESSY
Beamline	BL14-1	I911-5	I02	BL14-2	ID14-4	BL14-1	BL14-2
Wavelength (Å)	0.91841	0.90770	0.97950	0.91841	0.93928	0.91841	0.93928
Space group	$P4_32_12$	$P3_221$	$P2_12_12_1$	$P2_12_12_1$	$P222_1$	$P222_1$	$C222_1$
Unit cell dimensions							
a (Å)	71.36	66.35	33.71	32.95	46.62	46.60	68.10
b (Å)	71.36	66.35	41.07	41.25	59.94	60.03	91.19
c (Å)	71.44	110.69	108.92	108.54	144.34	145.07	62.85
α (°)	90	90	90	90	90	90	90
β (°)	90	90	90	90	90	90	90
γ (°)	90	120	90	90	90	90	90
Resolution (Å)	35.0–2.20 (2.26–2.20)	30.0–2.20 (2.30–2.20)	35.0–1.15 (1.18–1.15)	35.0–1.60 (1.64–1.60)	30.0–2.80 (2.87–2.80)	50.0–2.00 (2.05–2.00)	35.0–2.20 (2.26–2.20)
No. of unique reflections	9,427 (667)	14,842 (1,824)	53,461 (3,305)	18,999 (1,331)	10,295 (750)	28,298 (2,043)	10,255 (740)
R_{merge} (%)[a]	9.3 (62.3)	14.9 (58.4)	5.3 (43.4)	4.2 (26.8)	12.1 (74.4)	6.3 (66.7)	12.7 (55.3)
Completeness (%)	99.8 (99.7)	99.9 (99.9)	97.8 (82.7)	93.7 (64.5)	99.9 (99.7)	99.9 (99.9)	100 (100)
Redundancy	11.8 (12.2)	9.0 (9.1)	6.7 (4.9)	13.7 (10.9)	8.3 (7.6)	7.1 (6.9)	7.2 (7.2)
<I/σI>	26.6 (6.8)	14.0 (4.2)	20.9 (3.9)	43.8 (9.6)	10.1 (2.3)	24.6 (3.2)	13.9 (4.4)
Phasing							
MR starting model	1SPV	3IID	–	3V2B	3Q6Z, 3Q71	–	1SPV
Refinement							
Resolution (Å)	31.9–2.23	28.7–2.20	32.8–1.15	32.8–1.60	46.6–2.80	39.2–2.00	34.0–2.20
R_{all} (%)[b]	21.18	19.09	16.22	16.83	23.79	19.93	17.87
R_{free} (%)[b]	27.84	22.27	19.13	20.64	28.31	23.82	24.09
Rmsd bond length (Å)	0.018	0.010	0.017	0.015	0.013	0.012	0.017
Rmsd bond angle (°)	1.8	1.3	1.6	1.5	1.5	1.3	1.9
Ramachandran plot [c]							
Favored (%)	97.3	98.5	98.3	98.3	94.3	98.4	97.2
Allowed (%)	100	100	100	100	100	100	100

Values in parentheses are for the outermost resolution shell. See also Table S2.

[a] $R_{merge} = \sum |I - \langle I \rangle| / \sum I$, where I is the intensity measurement for a given reflection, and $\langle I \rangle$ is the average intensity for multiple measurements of this reflection.

[b] $R = \sum ||F_{obs}| - |F_{calc}|| / \sum |F_{obs}|$, where R_{free} is calculated for a randomly chosen 5%–10% of reflections, which were not used for structure refinement, and R_{all} is calculated for all reflections.

[c] The Ramachandran plot was calculated using the MolProbity server (http://molprobity.biochem.duke.edu/) (Davis et al., 2007).

automodification site might be a reason for the altered binding of Macro2 and Macro3, i.e., Macro3 bound more efficiently in vitro and Macro2 in cells to automodified ARTD10 (Figures 1 and 5). It is conceivable that these two macrodomains interact preferentially with distinct MARylated sites on ARTD10, which might be differentially modified in vivo and in vitro. This could be the result of interacting proteins in cells that are not present in the in vitro assays with purified components. This differential binding may also reflect that the two macrodomains recognize MARylation in slightly different contexts. Either the underlying peptide sequence and/or structural differences of the individual sites are likely to contribute to the interaction. The findings that ADPr is a rather poor competitor for binding of macrodomains to automodified ARTD10 (Figures 2B and S1D) and that neither Macro2 nor Macro3 binds to poly-ADP-ribosylated ARTD1 (Figure 1F) support this conclusion. Also notable is that the endogenous ARTD10 only colocalizes to a certain extent with Macro1–3, especially if the expression was not enhanced by IFN-α treatment. One explanation might be that only a subpopulation of ARTD10 is active in cells, and/or stimuli are required to enhance the catalytic activity.

In signaling events, specific recognition of modified target proteins by a reader domain is essential (Hunter, 2007). Additionally, combinatorial effects are key to define specificity and stability of interactions, potentially requiring the correct spatial orientation of specific reader domains and/or combinations of posttranslational modifications. As an example, recruitment of the NURF complex to chromatin depends on the correct alignment of the PHD finger and the bromodomains of BPTF, which recognize H3K4me2/H3K4me3 and H4K16ac,

Table 2. ITC to Determine the ADPr-Binding Properties of ARTD8 Macrodomain Protein Constructs

	K_D^{app} (μM); ITC		
ARTD8 Construct Protein	First	Second	Third
Macrodomain 1	192 ± 7	–	–
Macrodomain 2	6.0 ± 0.1	–	–
Macrodomain 3	1.9 ± 0.1	–	–
Macrodomain 1+2[a]	6.4 ± 0.2	261 ± 30	–
Macrodomain 2+3[a]	1.84 ± 0.45	12.6 ± 0.9	–
Macrodomain 1+2+3[a]	1.2 ± 0.04	18.7 ± 0.3	273 ± 4.3

See also Figure S2 and Table S1.
[a]Experimental data were fitted to an independent-site model (n = 1).

respectively (Ruthenburg et al., 2011). Thus, an important question to address in the future is whether the ARTD8 macrodomains and the WWE domain cooperate in recognizing interaction partners and substrates. The fundamental finding of a tool to investigate MARylation by ARTD10 will allow future studies to define endogenous ARTD10 substrates and to address the physiological relevance, for example for Ran, of MARylation.

EXPERIMENTAL PROCEDURES

Molecular Cloning

All ARTD10 (PARP10) constructs have been described previously (Kleine et al., 2008). The cDNAs encoding human ARTD8/BAL2 (Q460N5) and ARTD7/BAL3 (Q460N3) were obtained from the National Institute of Technology and Evaluation, Japan (accession number AK304269) and the Mammalian Gene Collection (accession number BC101701), respectively. The X-ray crystallography and ITC experiments, the regions encoding ARTD8 residues Gly789–Lys979 (macrodomain-1; hereafter called Macro1), Gly999–Ser1196 (Macro2), Phe1208–Gly1388 (Macro3), Gly784–Ser1196 (Macro12), Ala994–Gly1388 (Macro23), Ser794–Ser1393 (Macro123), and ARTD7 residues Thr272–Asn448 (ARTD7-Macro2) were amplified by PCR and inserted into bacterial expression vector pNIC28-Bsa4 by ligation-independent cloning (Gileadi et al., 2008). All expression constructs encoded an N-terminal hexahistidine tag separated from the target protein by a tobacco etch virus (TEV) protease cleavage site. For additional clonings, see Supplemental Experimental Procedures.

Antibodies

We purchased antibodies specific for GFP (600-301-215; Rockland), Ran (ab13049; Abcam), Flag (M2; Sigma-Aldrich), ARTD1 (1835238; Roche), PAR (10H, 1020; Tulip Biolabs), GAPDH (4G5, MCA4740; AbD Serotec), and Actin (C4; MP Biomedicals). The ARTD10-specific antibody is a purified polyclonal serum derived from rabbit immunized with the ARTD10(206–255) fragment.

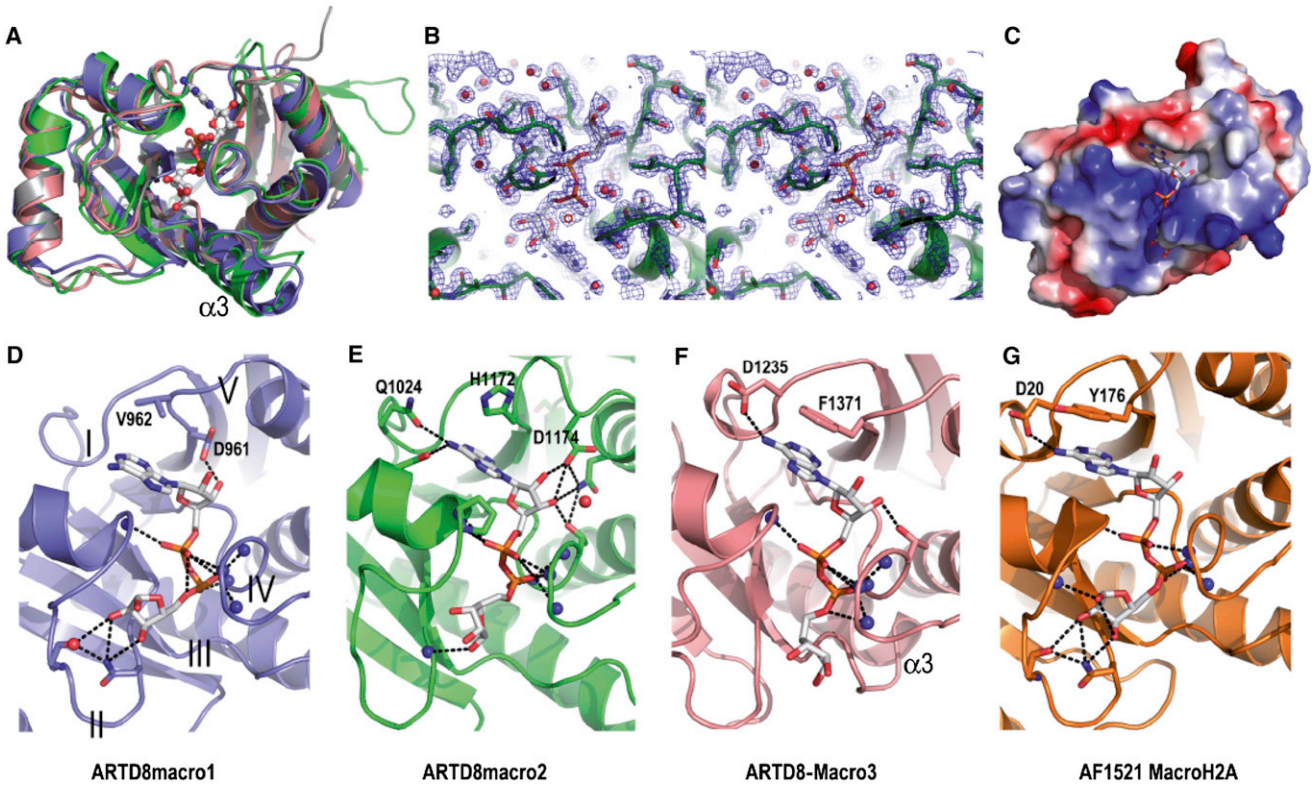

Figure 4. ADPr Binding of ARTD8 Macrodomains

(A) Superposition of the crystal structures of individual ADPr-bound ARTD8 macrodomains 1 (blue), 2 (green), and 3 (salmon), as well as ARTD7 macrodomain 2 (gray).

(B) Stereo image of the electron density ($2F_{obs}-F_{calc}$ map calculated using REFMAC5 [Murshudov et al., 2011] and rendered at 1.8σ) and the resulting model for the ligand-binding site in Macro3.

(C) Surface of Macro3 rendered to illustrate the ADPr-binding grove and surrounding charge distribution.

(D–G) Details of the interactions between protein and ADPr as seen in the crystal structures of ARTD8 Macro1 (D), ARTD8 Macro2 (E), ARTD8 Macro3 (F), and histone macroH2A domain of AF1521 (PDB 2BQF) (G).

See also Figures S3 and S4.

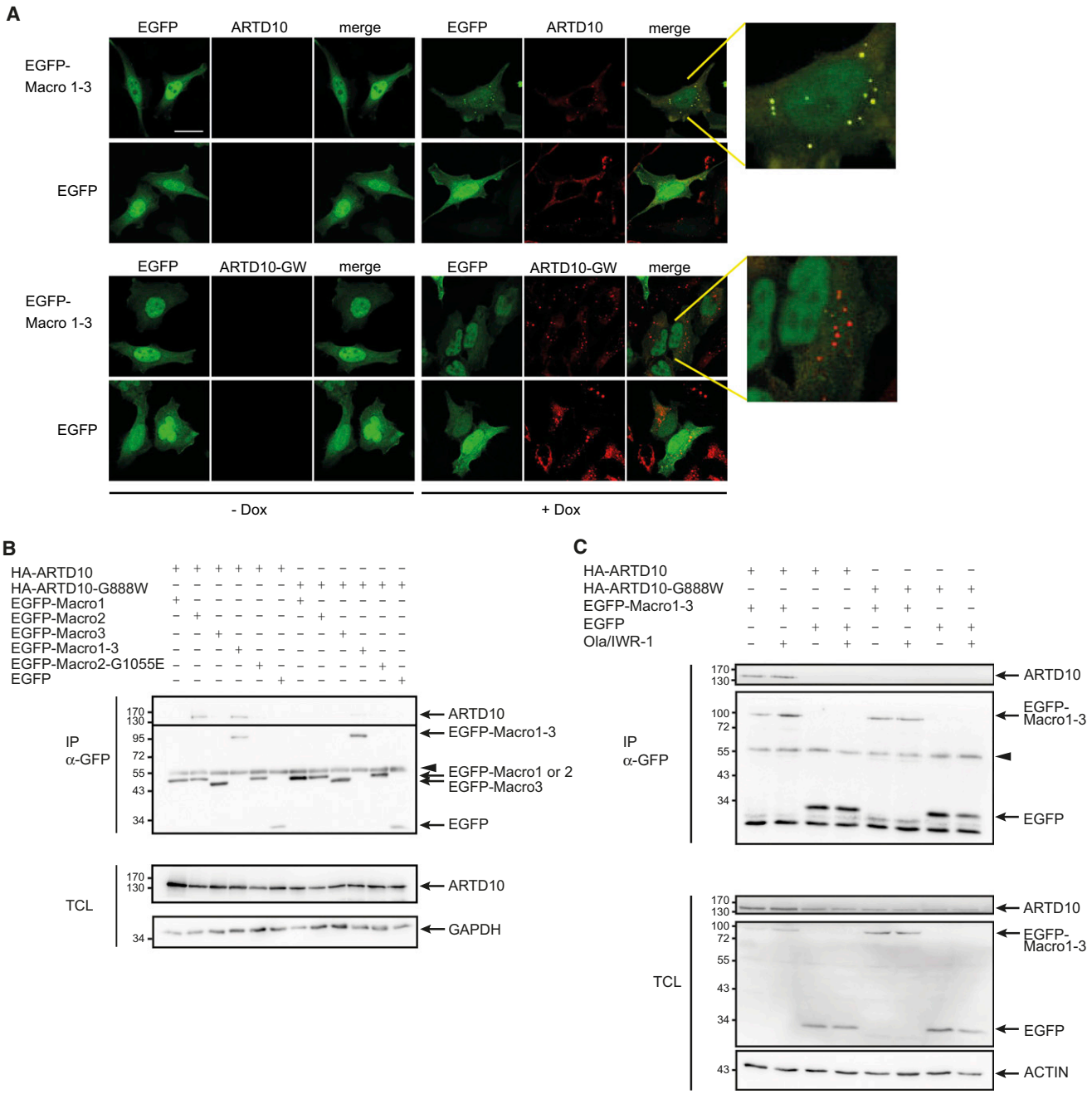

Figure 5. Artd8 Macrodomains Interact with ARTD10 in Cells

(A) HeLa cells stably expressing inducible ARTD10 or ARTD10-G888W were transiently transfected with EGFP-Macro1–3. The localization of EGFP-Macro1–3 and ARTD10 before and after induction was analyzed by confocal microscopy. Scale bar, 20 μM. The panels on the right show enlargements of the indicated merged images.

(B) HA-ARTD10, HA-ARTD10-G888W, and the indicated EGFP-fusion proteins were expressed transiently in HEK293 cells. The cells were then lysed and EGFP-containing complexes immunoprecipitated (IP). ARTD10 associated with the different EGFP-fusion proteins were analyzed by western blot analysis (mAb 5H11, upper panel). The different EGFPs are shown in the lower panel. TCL, total cell lysates with expression of ARTD10 and GAPDH as control. The arrowhead identifies a nonspecific band.

(C) The experiment was carried out as in (B). The indicated samples were treated with 2 μM IWR-1 for 24 hr and with 10 μM Olaparib for 2 hr prior to cell lysis. The arrowhead identifies a nonspecific band.

See also Figures S5, S6, and S8.

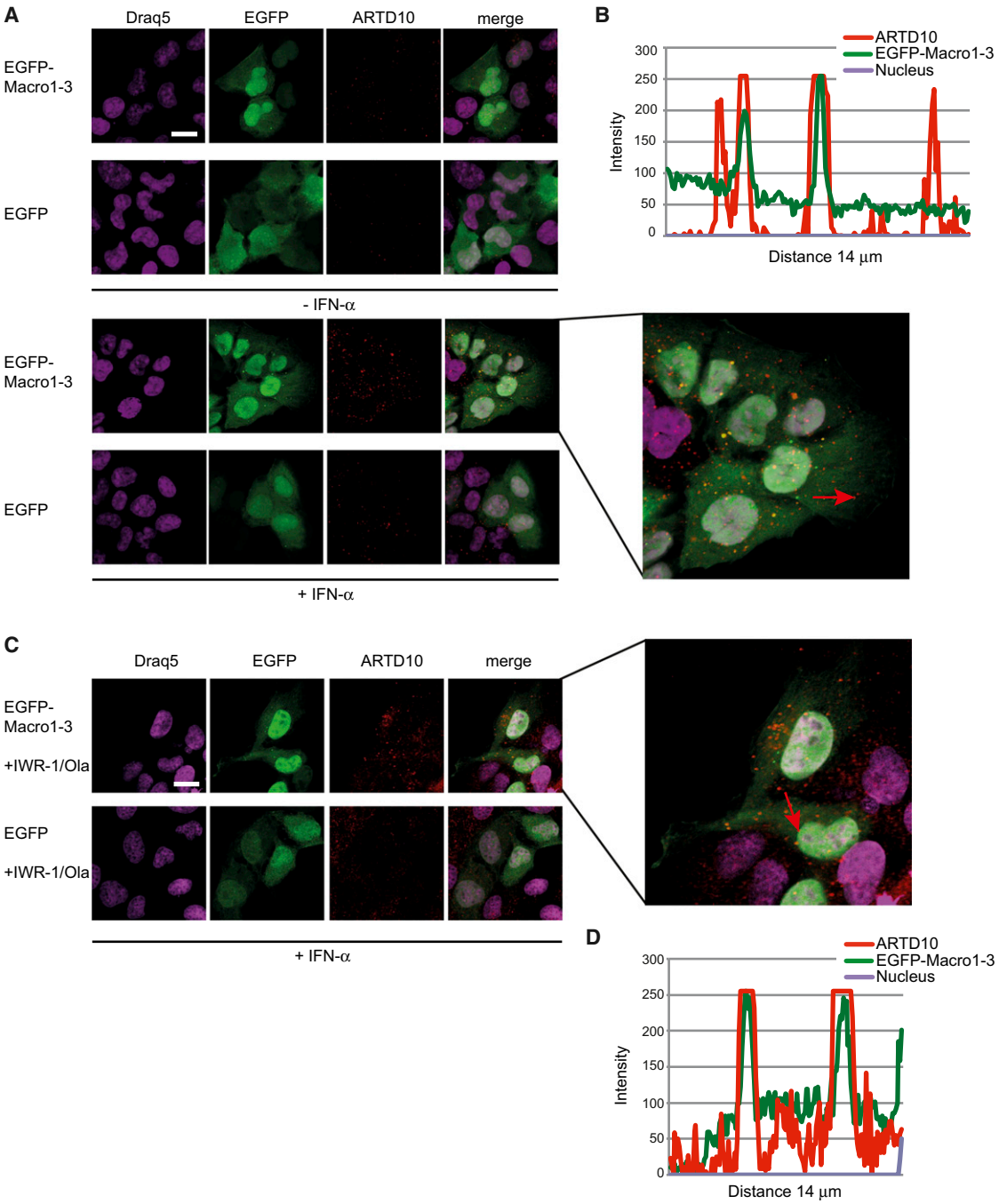

Figure 6. Artd8 Macrodomains Colocalize with Endogenous ARTD10 in Cells

(A) U2OS cells were transiently transfected with EGFP or EGFP-Macro1–3. The indicated samples were treated with IFN-α for 24 hr. ARTD10 was stained using polyclonal antibodies and secondary antibodies coupled to Alexa Fluor 555. Nuclei were stained with Draq5. Colocalization with and without IFN-α treatment was analyzed by confocal microscopy. Scale bar, 20 μM. An enlargement of the displayed merge picture is shown on the right. The red arrow specifies the location of the colocalization profile shown in (B).

(B) Colocalization profile of ARTD10 and EGFP-Macro1–3. The distance of 14 μM corresponds to the length of the red arrow in (A).

(C) The experimental setup was as in (A) with the exception that the indicated samples were treated with 2 μM IWR-1 for 24 hr and with 10 μM Olaparib for 2 hr before fixation and staining of the cells.

(D) Colocalization profile of ARTD10 and EGFP-Macro1–3 after inhibitor treatment. The distance of 14 μM is represented by the red arrow in the enlargement in (C).

See also Figures S6–S8.

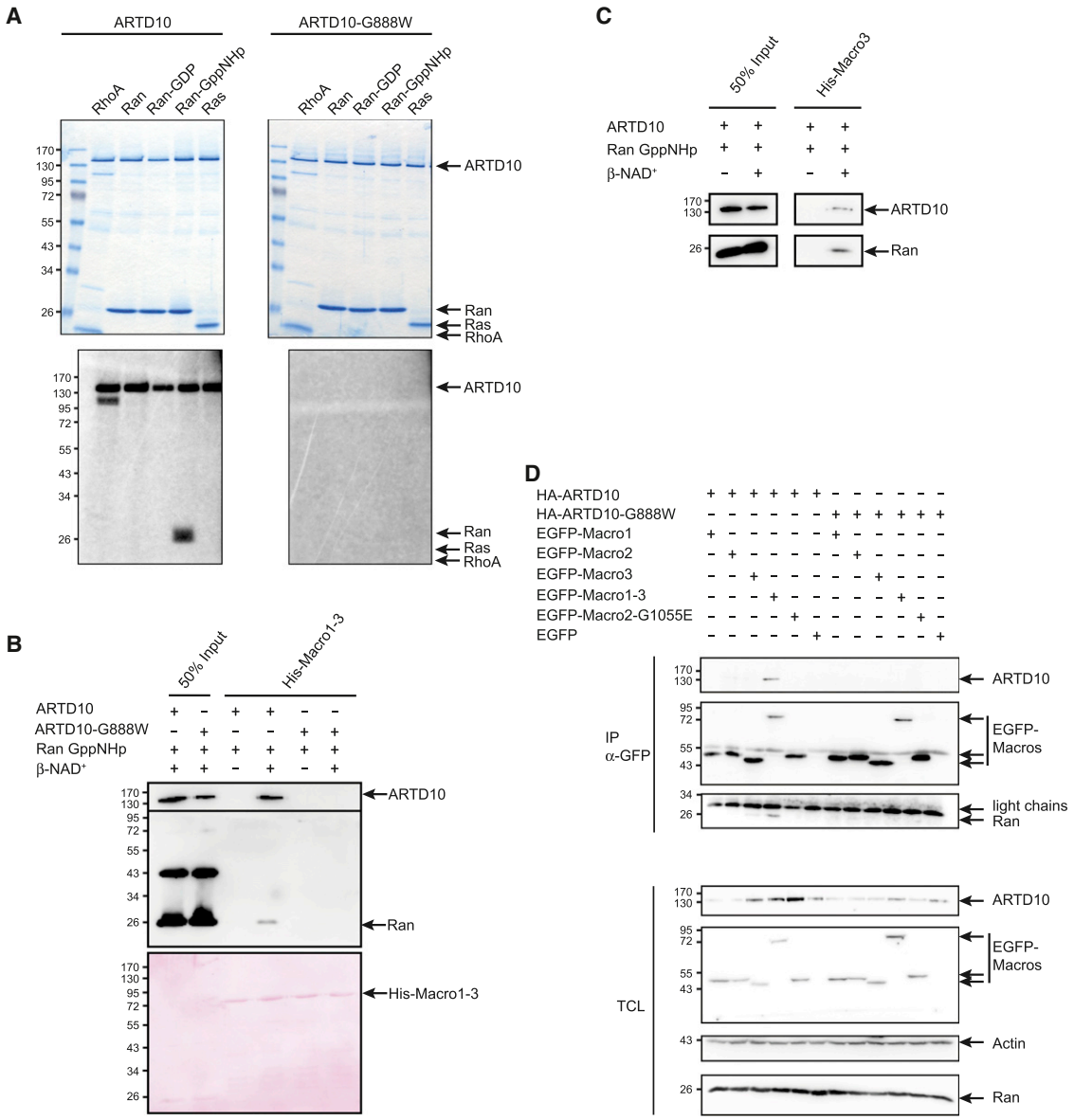

Figure 7. Artd8 Macrodomains Interact with Mono-ADP-Ribosylated Ran, an ARTD10 Substrate

(A) The indicated bacterially expressed GTPases (Ran, Ras, and Rho) were used as substrates in ADP-ribosylation assays with ^{32}P-β-NAD$^+$. Ran was either unloaded or loaded with GDP or GppNHp, a nonhydrolyzable GTP analog. The upper panels show Coomassie blue-stained gels, the lower panels autoradiographs.

(B and C) Ran-GppNHp was incubated with ARTD10 or ARTD10-G888W in the presence or absence of 500 μM β-NAD$^+$. The interaction of ARTD10 and Ran with His-Macro1–3 (B) and His-Macro3 (C) was determined by western blot analysis. For control, the blot was stained with Ponceau red (lower panel in B).

(D) HA-ARTD10 or HA-ARTD10-G888W was expressed transiently together with the indicated EGFP-fusion proteins in HEK293 cells. Upon lysis, the EGFP-fusion proteins were immunoprecipitated with specific antibodies, and the bound proteins were analyzed by western blotting (upper panel). For control, the expressed proteins and endogenous Ran and actin were stained (lower panel).

The monoclonal antibody 5H11 of rat IgG subclass recognizes ARTD10(300–350). The GST-specific antibody is a monoclonal antibody derived from a rat immunized with GST (mAb 6G9).

Macrodomain His-/GST-Pull-Down Experiments

All His-/GST-tagged proteins were purified using standard protocols as described in the Supplemental Experimental Procedures. A total of 5 μg of purified His-tagged macrodomains was preincubated with 25 μl equilibrated TALON Metal Affinity Resin (BD Biosciences) in 350 μl IMAC lysis/wash buffer containing 10 mM imidazole at 4°C for 2 hr. Afterward, the beads were washed twice with ice-cold IMAC lysis/wash buffer. ADP-ribosyltransferase assays were performed in 30 μl ADPr buffer (50 mM Tris [pH 8.0], 0.2 mM DTT, and 4 mM $MgCl_2$) and 500 μM β-NAD$^+$ with 0.5 μg TAP-purified ARTD10 or ARTD10-G888W under permanent agitation at 30°C for 30 min. Where applicable, 5 μg of GST-ARTD10(1–255) or 1 μg of the respective Ran-GTPase as a substrate was added to the ADPr assay. The general

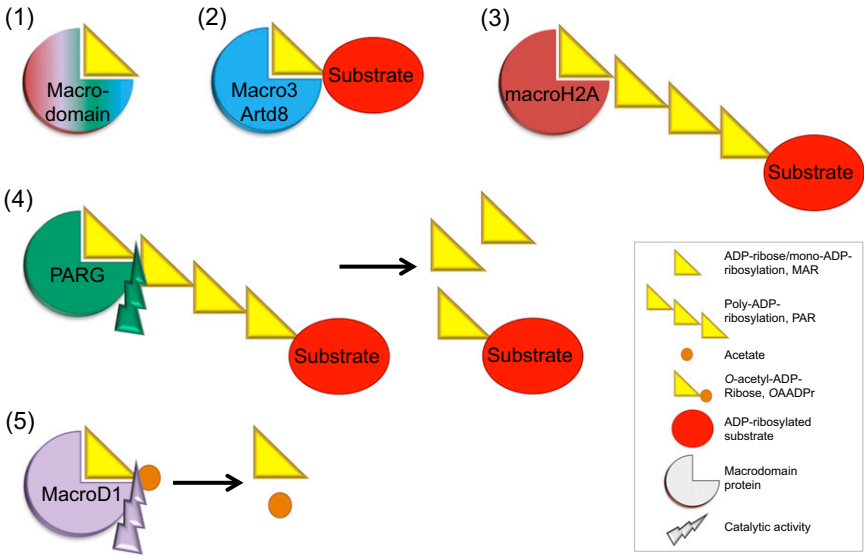

Figure 8. Summary of Macrodomain Functions

Scheme illustrating binding or catalytic properties of different macrodomain types. One representative for each type is indicated: (1) as a common feature, most macrodomains bind ADPr, albeit with variable affinities; (2) binding of MARylated proteins; (3) binding of PARylated proteins; (4) hydrolysis of PAR chains; and (5) hydrolysis of *O*AADPr.

ADP-ribosyltransferase inhibitor benzamide was added to the ADPr assay at the indicated concentrations. Then the ADPr assays were incubated with the TALON Metal Affinity Resin and the prebound macrodomains at 4°C for 2 hr, together with 350 μl IMAC lysis/wash buffer and 10 mM imidazole. In the samples with Ran-GppNHp, 20 mM imidazole was included. Western blots were evaluated using the Fujifilm LAS-3000 imaging system and processed using Adobe Photoshop.

A total of 5 μg of GST or GST-tagged macrodomain or WWE-domain proteins of Artd8 or GST-tagged macroH2A1.1(162–369) proteins was preabsorbed onto 25 μl of glutathione Sepharose (Sigma-Aldrich) in the presence of 350 μl pull-down buffer (100 mM Tris-HCl [pH 7.6], 250 mM NaCl, 50 mM KCl, 5 mM $MgCl_2$, 0.5% NP-40, 1 mM DTT, 0.5 mM EDTA, 10% glycerol, and protease inhibitors) at 4°C for 2 hr. An ADPr assay with 0.5 μg TAP-purified ARTD10 or 0.3 μg baculo-derived His-purified ARTD1 in the absence or presence of 50 μM or 500 μM β-NAD^+ was performed as described above. Next, modified or unmodified ARTD10 or ARTD1 was incubated with the WWE/macrodomain-glutathione Sepharose beads in 350 μl of pull-down buffer. Complexes were subsequently analyzed by western blotting with specific antibodies.

Purification of TAP-Tagged ARTD10/ARTD10-G888W and Enzymatic ADP-Ribosyltransferase Assays

The purification of ARTD10 and mutants and the enzymatic ADP-ribosyltransferase assays were performed as described before (Kleine et al., 2008).

Equipment and Settings for Immunofluorescence Microscopy

Cells were fixed by 3.8% paraformaldehyde, permeabilized with 0.1% Triton X-100 in PBS, and blocked by preincubation in PBS containing 0.1% Triton X-100 and 1% BSA at room temperature for 30 min. Fixed cells were stained with antibodies specific for the Flag epitope (M2) or for ARTD10 (mAb 5H11), diluted 1:100 in PBS containing 0.2% BSA (PBS/BSA) at 37°C for 1 hr. Further details are given in the Supplemental Experimental Procedures.

Immunofluorescence images were captured by a Zeiss Axiovert 100 M confocal laser-scanning microscope (LSM 510) or a Zeiss LSM 710 laser-scanning microscope. All details are given in the Supplemental Experimental Procedures.

Coimmunoprecipitations

HEK293 cells were transiently cotransfected with constructs expressing EGFP-tagged macrodomains and HA-ARTD10 or HA-ARTD10-G888W as indicated using the calcium phosphate coprecipitation method (Bousset et al., 1994). Forty-eight hours after transfection, cells were harvested and lysed in TAP-lysis buffer (Kleine et al., 2008). EGFP-fusion proteins were immunoprecipitated, and the bound proteins were analyzed by western blots using the indicated antibodies. For experiments where the inhibitors Olaparib and IWR-1 were used, cells were treated with 2 μM of IWR-1 24 hr after transfection for the following 24 hr. Olaparib was added to the cells at a concentration of 10 μM for 2 hr before lysis of the cells.

The functionality of Olaparib was tested by treating HEK293 cells with or without 2 μM of IWR-1 for 24 hr and 10 μM Olaparib for 2 hr. ARTD1 was induced in the indicated samples by addition of 1 mM H_2O_2 for 10 min. Subsequently, cells were lysed in sample buffer, and western blot analysis with specific PAR antibodies (10H) was performed.

Protein Purification for Crystallization and ITC Experiments

Amino-terminal hexahistidine fusions of human macrodomain protein constructs were expressed in *E. coli* and purified using standard methodology, as detailed in the Supplemental Experimental Procedures.

Crystallization

Crystals were grown by the sitting drop vapor diffusion method. Where applicable, ligands were preincubated with the protein solutions prior to setting up drops. Details of the crystallization conditions are summarized in Table S2.

Data Collection, Phasing, and Refinement

Crystals were transferred to a cryoprotectant solution (well solution supplemented with either glycerol or butanediol) and cooled and stored in liquid nitrogen. Details on data collection, phasing using molecular replacement, refinement procedures, and statistics are given in Table 1. Data were indexed and integrated using the XDS package (Kabsch, 2010) or the autoPROC toolbox (Vonrhein et al., 2011). Balbes (Nichols et al., 2008) or MOLREP (Vagin and Teplyakov, 2010) was used for molecular replacement. Model building was done with Coot (Emsley et al., 2010) and refinement with REFMAC5 (Murshudov et al., 2011). The refinement progress was monitored by decreasing R and R_{free} values.

The structure of ARTD8-Macro2 (3Q71) featured an extended β-loop-β structure, formed partially from residues in the hexahistidine affinity tag, at the N terminus. This motif has not been observed in any other macrodomain structure and is likely a cloning artifact.

ITC

ARTD8 macrodomain proteins were dialyzed overnight in 20 mM HEPES (pH 7.5), 300 mM NaCl, 10% glycerol, and 2 mM TCEP. Protein concentration after dialysis was determined using extension coefficients calculated from the protein construct sequences. ITC was performed at 25°C using an ITC200 microcalorimeter (MicroCal; GE Healthcare Life Sciences). A protein solution (39–50 μM) was loaded into the sample cell and titrated with ADPr (0–500 μM) at a stirring rate of 1,000 rpm. Results were analyzed with Origin software (MicroCal). The observed values for binding enthalpy were corrected for heat of dilution of ligand into the buffer and fitted to one-site and independent-site-binding models, as indicated in Tables 2 and S1.

ACCESSION NUMBERS

Coordinates have been deposited into the Protein Data Bank with accession codes 3Q6Z (ARTD8 macrodomain-1 ADPr complex), 3Q71 (ARTD8 macrodomain-2 ADPr complex), 4ABL (ARTD8 macrodomain-3 *apo* protein), 4ABK (ARTD8 macrodomain-3 ADPr complex), 3VFQ (ARTD8 macrodomain-1 *apo*, macrodomain-2 ADPr complex), 4D86 (ARTD8 macrodomain-1 ADP, macrodomain-2 ADP complex), and 3V2B (ARTD7 macrodomain-2 ADPr complex).

SUPPLEMENTAL INFORMATION

Supplemental Information includes eight figures, two tables, and Supplemental Experimental Procedures and can be found with this article online at http://dx.doi.org/10.1016/j.str.2012.12.019.

ACKNOWLEDGMENTS

We thank the staff at the BESSY (Berlin), MAX-Lab (Lund, Sweden), ISA (Aarhus, Denmark), ESRF (Grenoble, France), and Diamond (Oxfordshire, UK) synchrotron radiation facilities for excellent technical support. We thank Alfred Wittinghofer (MPI Dortmund) for providing the purified GTPases, Stephen Taylor (University of Manchester) for providing the FlpIn-HeLa cells, Michael Hottiger for providing the purified ARTD1, and Ida Johansson, Tine Kragh-Nielsen, Barbara Lippok, and Linda Svensson for technical assistance. The Structural Genomics Consortium is a registered charity (1097737) that receives funds from Sweden, UK, and Canada (http://www.thesgc.org/openaccess/funders//). H.S. acknowledges additional support from the Swedish Foundation for Strategic Research (grant RBc08-0014). Structural data collection was supported by the European Community Seventh Framework Programme (FP7/2007-2013) under grant agreement #226716. The work was supported by a grant from the German Research Foundation DFG and a START grant from the Medical School of the RWTH Aachen University to B.L.

A.F. performed the majority of the experiments, evaluated data, and wrote the manuscript. T.K. conducted crystallization experiments, solved the crystal structures, and evaluated data. N.H. established the stable HeLa cell lines. K.L.H.F. and P.V. purified ARTD10 and ARTD10-G888W. A.G. identified IFN-α as inducer of ARTD10. A.-G.T. conducted crystallization experiments and purified protein. P.K. conducted structural analysis. B.N. conducted ITC experiments. H.K. provided conceptual input and performed in vitro GTPase experiments. E.K. prepared monoclonal antibodies. A.L. evaluated data. H.S. and B.L. supervised the research, conducted experiments, evaluated data, and wrote the manuscript.

Received: October 23, 2012
Revised: December 13, 2012
Accepted: December 21, 2012
Published: February 28, 2013

REFERENCES

Aguiar, R.C., Yakushijin, Y., Kharbanda, S., Salgia, R., Fletcher, J.A., and Shipp, M.A. (2000). BAL is a novel risk-related gene in diffuse large B-cell lymphomas that enhances cellular migration. Blood *96*, 4328–4334.

Aguiar, R.C., Takeyama, K., He, C., Kreinbrink, K., and Shipp, M.A. (2005). B-aggressive lymphoma family proteins have unique domains that modulate transcription and exhibit poly(ADP-ribose) polymerase activity. J. Biol. Chem. *280*, 33756–33765.

Ahel, I., Ahel, D., Matsusaka, T., Clark, A.J., Pines, J., Boulton, S.J., and West, S.C. (2008). Poly(ADP-ribose)-binding zinc finger motifs in DNA repair/checkpoint proteins. Nature *451*, 81–85.

Altmeyer, M., Messner, S., Hassa, P.O., Fey, M., and Hottiger, M.O. (2009). Molecular mechanism of poly(ADP-ribosyl)ation by PARP1 and identification of lysine residues as ADP-ribose acceptor sites. Nucleic Acids Res. *37*, 3723–3738.

Andrabi, S.A., Kang, H.C., Haince, J.F., Lee, Y.I., Zhang, J., Chi, Z., West, A.B., Koehler, R.C., Poirier, G.G., Dawson, T.M., and Dawson, V.L. (2011). Iduna protects the brain from glutamate excitotoxicity and stroke by interfering with poly(ADP-ribose) polymer-induced cell death. Nat. Med. *17*, 692–699.

Bousset, K., Oelgeschläger, M.H., Henriksson, M., Schreek, S., Burkhardt, H., Litchfield, D.W., Lüscher-Firzlaff, J.M., and Lüscher, B. (1994). Regulation of transcription factors c-Myc, Max, and c-Myb by casein kinase II. Cell. Mol. Biol. Res. *40*, 501–511.

Callow, M.G., Tran, H., Phu, L., Lau, T., Lee, J., Sandoval, W.N., Liu, P.S., Bheddah, S., Tao, J., Lill, J.R., et al. (2011). Ubiquitin ligase RNF146 regulates tankyrase and Axin to promote Wnt signaling. PLoS One *6*, e22595.

Chen, B., Dodge, M.E., Tang, W., Lu, J., Ma, Z., Fan, C.W., Wei, S., Hao, W., Kilgore, J., Williams, N.S., et al. (2009). Small molecule-mediated disruption of Wnt-dependent signaling in tissue regeneration and cancer. Nat. Chem. Biol. *5*, 100–107.

Chen, D., Vollmar, M., Rossi, M.N., Phillips, C., Kraehenbuehl, R., Slade, D., Mehrotra, P.V., von Delft, F., Crosthwaite, S.K., Gileadi, O., et al. (2011). Identification of macrodomain proteins as novel O-acetyl-ADP-ribose deacetylases. J. Biol. Chem. *286*, 13261–13271.

Dani, N., Stilla, A., Marchegiani, A., Tamburro, A., Till, S., Ladurner, A.G., Corda, D., and Di Girolamo, M. (2009). Combining affinity purification by ADP-ribose-binding macro domains with mass spectrometry to define the mammalian ADP-ribosyl proteome. Proc. Natl. Acad. Sci. USA *106*, 4243–4248.

Dani, N., Mayo, E., Stilla, A., Marchegiani, A., Di Paola, S., Corda, D., and Di Girolamo, M. (2011). Mono-ADP-ribosylation of the G protein betagamma dimer is modulated by hormones and inhibited by Arf6. J. Biol. Chem. *286*, 5995–6005.

Davis, I.W., Leaver-Fay, A., Chen, V.B., Block, J.N., Kapral, G.J., Wang, X., Murray, L.W., Arendall, W.B., 3rd, Snoeyink, J., Richardson, J.S., and Richardson, D.C. (2007). MolProbity: all-atom contacts and structure validation for proteins and nucleic acids. Nucleic Acids Res. *35*(Web Server issue), W375–W383.

Di Girolamo, M., Dani, N., Stilla, A., and Corda, D. (2005). Physiological relevance of the endogenous mono(ADP-ribosyl)ation of cellular proteins. FEBS J. *272*, 4565–4575.

Di Paola, S., Micaroni, M., Di Tullio, G., Buccione, R., and Di Girolamo, M. (2012). PARP16/ARTD15 is a novel endoplasmic-reticulum-associated mono-ADP-ribosyltransferase that interacts with, and modifies karyopherin-ß1. PLoS One *7*, e37352.

Emsley, P., Lohkamp, B., Scott, W.G., and Cowtan, K. (2010). Features and development of Coot. Acta Crystallogr. D Biol. Crystallogr. *66*, 486–501.

Eustermann, S., Brockmann, C., Mehrotra, P.V., Yang, J.C., Loakes, D., West, S.C., Ahel, I., and Neuhaus, D. (2010). Solution structures of the two PBZ domains from human APLF and their interaction with poly(ADP-ribose). Nat. Struct. Mol. Biol. *17*, 241–243.

Gagné, J.P., Isabelle, M., Lo, K.S., Bourassa, S., Hendzel, M.J., Dawson, V.L., Dawson, T.M., and Poirier, G.G. (2008). Proteome-wide identification of poly(ADP-ribose) binding proteins and poly(ADP-ribose)-associated protein complexes. Nucleic Acids Res. *36*, 6959–6976.

Gibson, B.A., and Kraus, W.L. (2012). New insights into the molecular and cellular functions of poly(ADP-ribose) and PARPs. Nat. Rev. Mol. Cell Biol. *13*, 411–424.

Gileadi, O., Burgess-Brown, N.A., Colebrook, S.M., Berridge, G., Savitsky, P., Smee, C.E., Loppnau, P., Johansson, C., Salah, E., and Pantic, N.H. (2008). High throughput production of recombinant human proteins for crystallography. Methods Mol. Biol. *426*, 221–246.

Gottschalk, A.J., Timinszky, G., Kong, S.E., Jin, J., Cai, Y., Swanson, S.K., Washburn, M.P., Florens, L., Ladurner, A.G., Conaway, J.W., and Conaway, R.C. (2009). Poly(ADP-ribosyl)ation directs recruitment and activation of an ATP-dependent chromatin remodeler. Proc. Natl. Acad. Sci. USA *106*, 13770–13774.

Guetg, C., Scheifele, F., Rosenthal, F., Hottiger, M.O., and Santoro, R. (2012). Inheritance of silent rDNA chromatin is mediated by PARP1 via noncoding RNA. Mol. Cell *45*, 790–800.

Guettler, S., LaRose, J., Petsalaki, E., Gish, G., Scotter, A., Pawson, T., Rottapel, R., and Sicheri, F. (2011). Structural basis and sequence rules for substrate recognition by Tankyrase explain the basis for cherubism disease. Cell *147*, 1340–1354.

Hassler, M., Jankevicius, G., and Ladurner, A.G. (2011). PARG: a macrodomain in disguise. Structure *19*, 1351–1353.

Hottiger, M.O., Hassa, P.O., Lüscher, B., Schüler, H., and Koch-Nolte, F. (2010). Toward a unified nomenclature for mammalian ADP-ribosyltransferases. Trends Biochem. Sci. *35*, 208–219.

Huang, S.M., Mishina, Y.M., Liu, S., Cheung, A., Stegmeier, F., Michaud, G.A., Charlat, O., Wiellette, E., Zhang, Y., Wiessner, S., et al. (2009). Tankyrase inhibition stabilizes axin and antagonizes Wnt signalling. Nature *461*, 614–620.

Hunter, T. (2007). The age of crosstalk: phosphorylation, ubiquitination, and beyond. Mol. Cell *28*, 730–738.

Kabsch, W. (2010). Xds. Acta Crystallogr. D Biol. Crystallogr. *66*, 125–132.

Kang, H.C., Lee, Y.I., Shin, J.H., Andrabi, S.A., Chi, Z., Gagné, J.P., Lee, Y., Ko, H.S., Lee, B.D., Poirier, G.G., et al. (2011). Iduna is a poly(ADP-ribose) (PAR)-dependent E3 ubiquitin ligase that regulates DNA damage. Proc. Natl. Acad. Sci. USA *108*, 14103–14108.

Karras, G.I., Kustatscher, G., Buhecha, H.R., Allen, M.D., Pugieux, C., Sait, F., Bycroft, M., and Ladurner, A.G. (2005). The macro domain is an ADP-ribose binding module. EMBO J. *24*, 1911–1920.

Kleine, H., and Lüscher, B. (2009). Learning how to read ADP-ribosylation. Cell *139*, 17–19.

Kleine, H., Poreba, E., Lesniewicz, K., Hassa, P.O., Hottiger, M.O., Litchfield, D.W., Shilton, B.H., and Lüscher, B. (2008). Substrate-assisted catalysis by PARP10 limits its activity to mono-ADP-ribosylation. Mol. Cell *32*, 57–69.

Kleine, H., Herrmann, A., Lamark, T., Forst, A.H., Verheugd, P., Lüscher-Firzlaff, J., Lippok, B., Feijs, K.L., Herzog, N., Kremmer, E., et al. (2012). Dynamic subcellular localization of the mono-ADP-ribosyltransferase ARTD10 and interaction with the ubiquitin receptor p62. Cell Commun. Signal. *10*, 28.

Koch-Nolte, F., Kernstock, S., Mueller-Dieckmann, C., Weiss, M.S., and Haag, F. (2008). Mammalian ADP-ribosyltransferases and ADP-ribosylhydrolases. Front. Biosci. *13*, 6716–6729.

Kustatscher, G., Hothorn, M., Pugieux, C., Scheffzek, K., and Ladurner, A.G. (2005). Splicing regulates NAD metabolite binding to histone macroH2A. Nat. Struct. Mol. Biol. *12*, 624–625.

Levaot, N., Voytyuk, O., Dimitriou, I., Sircoulomb, F., Chandrakumar, A., Deckert, M., Krzyzanowski, P.M., Scotter, A., Gu, S., Janmohamed, S., et al. (2011). Loss of Tankyrase-mediated destruction of 3BP2 is the underlying pathogenic mechanism of cherubism. Cell *147*, 1324–1339.

Lupi, R., Corda, D., and Di Girolamo, M. (2000). Endogenous ADP-ribosylation of the G protein beta subunit prevents the inhibition of type 1 adenylyl cyclase. J. Biol. Chem. *275*, 9418–9424.

Mahmoud, L., Al-Saif, M., Amer, H.M., Sheikh, M., Almajhdi, F.N., and Khabar, K.S. (2011). Green fluorescent protein reporter system with transcriptional sequence heterogeneity for monitoring the interferon response. J. Virol. *85*, 9268–9275.

Murshudov, G.N., Skubák, P., Lebedev, A.A., Pannu, N.S., Steiner, R.A., Nicholls, R.A., Winn, M.D., Long, F., and Vagin, A.A. (2011). REFMAC5 for the refinement of macromolecular crystal structures. Acta Crystallogr. D Biol. Crystallogr. *67*, 355–367.

Nichols, K.P., Eijkel, J.C., and Gardeniers, H.J. (2008). Nanochannels in SU-8 with floor and ceiling metal electrodes and integrated microchannels. Lab Chip *8*, 173–175.

Pleschke, J.M., Kleczkowska, H.E., Strohm, M., and Althaus, F.R. (2000). Poly(ADP-ribose) binds to specific domains in DNA damage checkpoint proteins. J. Biol. Chem. *275*, 40974–40980.

Ruthenburg, A.J., Li, H., Milne, T.A., Dewell, S., McGinty, R.K., Yuen, M., Ueberheide, B., Dou, Y., Muir, T.W., Patel, D.J., and Allis, C.D. (2011). Recognition of a mononucleosomal histone modification pattern by BPTF via multivalent interactions. Cell *145*, 692–706.

Slade, D., Dunstan, M.S., Barkauskaite, E., Weston, R., Lafite, P., Dixon, N., Ahel, M., Leys, D., and Ahel, I. (2011). The structure and catalytic mechanism of a poly(ADP-ribose) glycohydrolase. Nature *477*, 616–620.

Tao, Z., Gao, P., and Liu, H.W. (2009). Identification of the ADP-ribosylation sites in the PARP-1 automodification domain: analysis and implications. J. Am. Chem. Soc. *131*, 14258–14260.

Timinszky, G., Till, S., Hassa, P.O., Hothorn, M., Kustatscher, G., Nijmeijer, B., Colombelli, J., Altmeyer, M., Stelzer, E.H., Scheffzek, K., et al. (2009). A macrodomain-containing histone rearranges chromatin upon sensing PARP1 activation. Nat. Struct. Mol. Biol. *16*, 923–929.

Vagin, A., and Teplyakov, A. (2010). Molecular replacement with MOLREP. Acta Crystallogr. D Biol. Crystallogr. *66*, 22–25.

Vetter, I.R., Nowak, C., Nishimoto, T., Kuhlmann, J., and Wittinghofer, A. (1999). Structure of a Ran-binding domain complexed with Ran bound to a GTP analogue: implications for nuclear transport. Nature *398*, 39–46.

Vonrhein, C., Flensburg, C., Keller, P., Sharff, A., Smart, O., Paciorek, W., Womack, T., and Bricogne, G. (2011). Data processing and analysis with the autoPROC toolbox. Acta Crystallogr. D Biol. Crystallogr. *67*, 293–302.

Wahlberg, E., Karlberg, T., Kouznetsova, E., Markova, N., Macchiarulo, A., Thorsell, A.G., Pol, E., Frostell, A., Ekblad, T., Öncü, D., et al. (2012). Family-wide chemical profiling and structural analysis of PARP and tankyrase inhibitors. Nat. Biotechnol. *30*, 283–288.

Wang, Z., Michaud, G.A., Cheng, Z., Zhang, Y., Hinds, T.R., Fan, E., Cong, F., and Xu, W. (2012). Recognition of the iso-ADP-ribose moiety in poly(ADP-ribose) by WWE domains suggests a general mechanism for poly(ADP-ribosyl)ation-dependent ubiquitination. Genes Dev. *26*, 235–240.

Yu, M., Schreek, S., Cerni, C., Schamberger, C., Lesniewicz, K., Poreba, E., Vervoorts, J., Walsemann, G., Grötzinger, J., Kremmer, E., et al. (2005). PARP-10, a novel Myc-interacting protein with poly(ADP-ribose) polymerase activity, inhibits transformation. Oncogene *24*, 1982–1993.

Zhang, Y., Liu, S., Mickanin, C., Feng, Y., Charlat, O., Michaud, G.A., Schirle, M., Shi, X., Hild, M., Bauer, A., et al. (2011). RNF146 is a poly(ADP-ribose)-directed E3 ligase that regulates axin degradation and Wnt signalling. Nat. Cell Biol. *13*, 623–629.